Sea surface temperature inter-hemispheric dipole and its relation to tropical precipitation

2013 Environ. Res. Lett. 8 044006

(http://iopscience.iop.org/1748-9326/8/4/044006)

OPEN ACCESS
IOP PUBLISHING
ENVIRONMENTAL RESEARCH LETTERS
Environ. Res. Lett. **8** (2013) 044006 (8pp)
doi:10.1088/1748-9326/8/4/044006

Sea surface temperature inter-hemispheric dipole and its relation to tropical precipitation

Cheng Sun[1], Jianping Li[1], Fei-Fei Jin[2] and Ruiqiang Ding[1]

[1] State Key Laboratory of Numerical Modeling for Atmospheric Sciences and Geophysical Fluid Dynamics (LASG), Institute of Atmospheric Physics, Chinese Academy of Sciences, Beijing, People's Republic of China
[2] Department of Meteorology, University of Hawaii at Manoa, Honolulu, HI 96822, USA

E-mail: ljp@lasg.iap.ac.cn

Received 31 July 2013
Accepted for publication 30 September 2013
Published 16 October 2013
Online at stacks.iop.org/ERL/8/044006

Abstract
Using different SST datasets, the variability of zonal mean SSTs is investigated. Besides the global warming mode, the variability is dominated by one equatorially symmetric mode and one antisymmetric mode. The former is most pronounced in the Pacific and dominated by interannual variability, corresponding to the ENSO signature. The latter features an inter-hemispheric dipole-like pattern and is referred to as the SST inter-hemispheric dipole (SSTID). The SSTID and Atlantic multidecadal oscillation are found to be related but distinct in the spatial pattern. Observational analysis shows that the SSTID significantly influences tropical rainfall and contributes to the north–south asymmetry of tropical precipitation on multidecadal timescales. The observed SSTID and its relation to the tropical rainfall are realistically reproduced in a control simulation with the UKMO-HadCM3 climate model. Results from the UKMO-HadCM3 simulation suggest that the SSTID is related to the variability of the global ocean northward cross-equatorial heat transport.

Keywords: global SST variability, SST inter-hemispheric dipole, thermal gradient, tropical rainfall

1. Introduction

There are latitudinally nonuniform changes in global surface temperature (Drost *et al* 2012). One of these latitudinal asymmetries is the difference in surface temperature warming trends between the Northern Hemisphere (NH) and Southern Hemisphere (SH), which has been attributed to the latitudinal asymmetry in the land–ocean fraction (Xu and Ramanathan 2012). Some studies have also revealed a difference in the evolution of NH and SH hemispheric mean sea surface temperature (SST), and have suggested an abrupt shift around the late 1960s, with cooling NH ocean and warming SH ocean (Baines and Folland 2007, Thompson *et al* 2010). Recent analyses with observation data and empirical orthogonal function (EOF) have described an inter-hemispheric asymmetric pattern of global SST (Dima and Lohmann 2010). However, its position in the EOF ranking is low (fourth or fifth) and varies depending on the SST datasets (Dima and Lohmann 2010). It has been suggested that such high-order EOFs tend to be subject to large uncertainty (Quadrelli *et al* 2005), and that they are difficult to reproduce and to interpret physically (Thompson *et al* 2010). Thus, there is still uncertainty regarding the dominant patterns of latitudinal SST changes. This paper investigates meridional modes of global SST variability by examining the leading

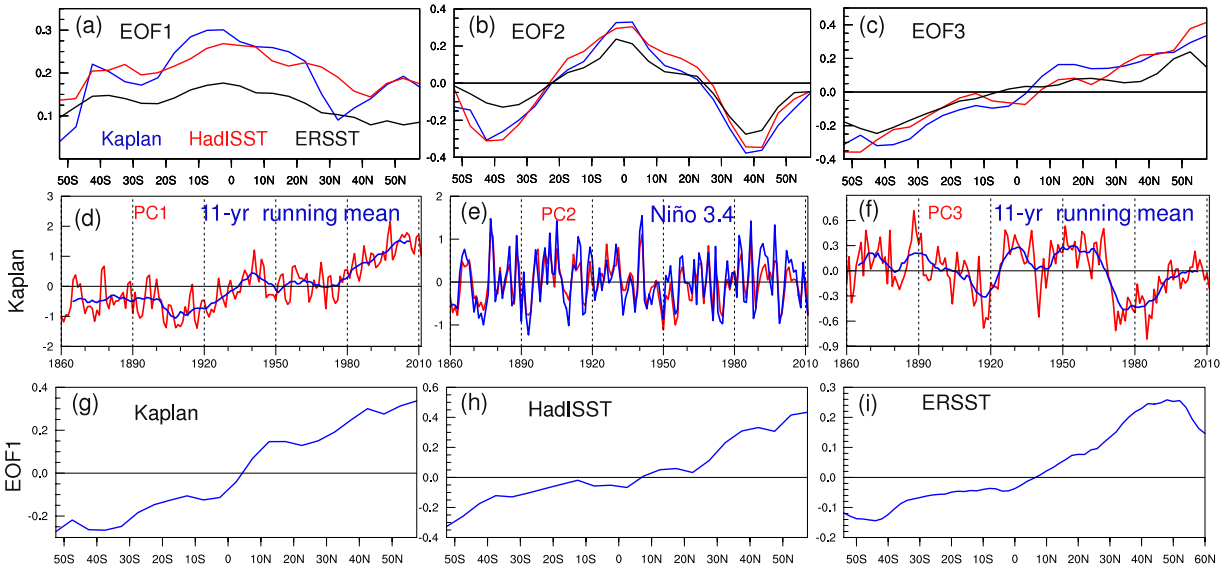

Figure 1. EOF1 (a), EOF2 (b) and EOF3 (c) of the annual zonal mean SSTA over the period 1860–2011 for the Kaplan (blue), HadISST (red), and ERSST (black) datasets. PCs corresponding to the EOF1 (d) and EOF3 (f) modes (red) and their 11-yr running means (blue) for Kaplan dataset. (e) The PC corresponding to the EOF2 mode (red) and the annual Niño 3.4 SSTA (blue). The EOF1 of the zonally averaged residual SST after removal of the global warming trend and the interannual ENSO signal for Kaplan (g), HadISST (h) and ERSST (i) datasets.

EOFs of zonally averaged SST, which can give us a view focusing on the meridional SST variation.

In this study, the long-term zonal mean SST variability is examined by analyzing an inter-hemispheric dipole mode. This mode shows an antiphase relationship for SST in the two hemispheres. It is partially associated with the Atlantic multidecadal oscillation (AMO; Enfield *et al* 2001, Knight *et al* 2005, Zhang *et al* 2013) but with clear difference in the spatial pattern. We investigate its relation to decadal variations in tropical precipitation and the underlying mechanisms.

2. Data and methods

The annual mean SST datasets (1860–2011) used in this study include the Hadley Centre SST dataset (HadISST, Rayner *et al* 2006), the extended reconstruction SST (ERSST) dataset (Smith and Reynolds 2005) from the NOAA Climate Diagnostics Center, and the Kaplan SST dataset (Kaplan *et al* 1998). Atmospheric data (1901–2009) are obtained from NOAA's 20th century reanalysis (Compo *et al* 2011), and include zonal wind, meridional wind and precipitable water (vertically integrated specific humidity). The precipitation data (1901–2009) are derived from the Climate Research Unit dataset (Mitchell and Jones 2005). All the datasets used in this study describe anomalies with respect to the base period 1961–1990. Annual mean SST and precipitation data from multi-centennial control simulations from a coupled ocean-atmospheric general circulation model, UKMO-HadCM3, were employed (downloaded from the Climate Model Inter-comparison Project 3 data portal). The UKMO-HadCM3 model was selected as it has realistic simulations of the observed ocean variability (Knight *et al* 2005, Guilyardi *et al* 2009). The control simulation from the UKMO-HadCM3 model spans 341 years and detailed descriptions of the model can be found in Gordon *et al* (2000).

In order to identify patterns of the latitudinal variations of global SST field, we performed EOF analysis on the zonal mean SST anomalies (SSTA). In the EOF analysis, area weighting is accomplished by multiplying zonal mean SST by the square root of cosine of latitude (North *et al* 1982a). The significance of the correlation between two auto-correlated time series was accessed via a two-tailed Student *t*-test using the effective number of degrees of freedom (Li *et al* 2012).

3. Results

3.1. Principal modes of zonal mean SSTA

Figures 1(a)–(c) show the latitudinal patterns of the first three leading EOF modes (hereafter EOF1, EOF2 and EOF3) of the annual zonal mean SSTA. For the Kaplan dataset, the first three modes account for 61%, 17% and 10% of the total variance, respectively (58%, 13% and 8% for HadISST, and 67%, 12% and 8% for ERSST). According to the criterion of North *et al* (1982b), EOF1, EOF2 and EOF3 are statistically distinguished from each other and the rest of the eigenvectors in terms of the sampling error bars (not shown). The EOF1 shows a latitudinally uniform-sign pattern, with strongest warming in tropical oceans and weak warming in extratropical oceans, and its principal component (PC1, shown in figure 1(d)) is dominated by a remarkable upward trend. Thus, the EOF1 mainly explains the SST warming trend, consistent with previous EOF analyses of the global SSTA (Parker *et al* 2007). The EOF2 is nearly symmetric about the equator, with warming in the tropics and cooling in both NH and SH extratropics during its positive phase.

Table 1. PC correlation coefficients between the Kaplan, HadISST and ERSST datasets for two periods: 1860–2011 and 1900–2011. (Note: all correlation coefficients are statistically significant at the 99% confidence level.)

		PC2			PC3		
		Kaplan	HadISST	ERSST	Kaplan	HadISST	ERSST
1860–2011(1900–2011)	Kaplan	1.00(1.00)	0.91(0.92)	0.88(0.92)	1.00(1.00)	0.77(0.84)	0.77(0.85)
	HadISST		1.00(1.00)	0.89(0.93)		1.00(1.00)	0.79(0.83)
	ERSST			1.00(1.00)			1.00(1.00)

The EOF3 is basically antisymmetric about the equator and represents antiphase SST fluctuations between the NH and SH, similar to the inter-hemispheric dipole mode obtained from EOF analysis of low-pass-filtered SSTA in previous studies (Folland *et al* 1999, Parker *et al* 2007). These previous analyses are mainly based on smoothed data using a filter passing decadal and longer-term variations, which might be incapable of revealing year-to-year SST variations. In our study, most of the year-to-year variability of latitudinal SST fluctuations can be decomposed into three principal modes: the global warming mode, one equatorially symmetric mode and one antisymmetric mode, and the latitudinal patterns of these three modes are almost the same in all three datasets. Figures 1(e) and (f) show the PCs corresponding to the EOF2 and EOF3 for Kaplan dataset. The annual PC2 and PC3 from different datasets are highly correlated over the long-term period (table 1), indicating that the temporal features of EOF2 and EOF3 are broadly consistent in all three datasets.

The PC2 time series (figure 1(e)) is dominated by interannual variability. The spatial pattern of EOF2 (figure 2(a)) is most pronounced over the Pacific basin and resembles that of El Niño–Southern oscillation (ENSO) with the highest loadings in tropical Pacific. This is different from the Pacific decadal oscillation which has maximum loadings in extratropical Pacific (Zhang *et al* 1997). The PC2 is strongly correlated with the annual Niño 3.4 (5°N–5°S, 170°–120°W) SSTA ($r = 0.88$ for 1860–2011) on interannual timescales, suggesting that the interannual variability of EOF2 can be largely attributed to ENSO. Previous studies have suggested that SST variations in other tropical ocean basins (e.g., Indian Ocean and tropical Atlantic) and extratropical ocean basins (e.g., North Pacific, South Pacific and North Atlantic) closely follow the ENSO variability, manifesting ENSO's remote impact through the atmospheric bridge (Alexander *et al* 2002, Deser *et al* 2010). Thus, the EOF2 in fact reflects the ENSO signature in global zonally averaged SST, which is basically symmetric about the equator.

The EOF3 shows an inter-hemispheric dipole-like pattern, and here it is referred to as the SST inter-hemispheric dipole (SSTID). If we filter out the global warming trend (defined as the global mean surface temperature Ting *et al* 2009) and the interannual ENSO signal from the raw SST data, the SSTID becomes the leading EOF of the zonal mean SSTs (shown in figures 1(g)–(i)). In this study, the SSTID is present in all the three SST datasets, and there is remarkable consistency (the correlations of the SSTID EOFs in HadISST and ERSST datasets with that in Kaplan dataset are 0.95 and 0.96, respectively), indicating that the SSTID is a real and robust feature of observed global SST variability. The corresponding PC3 time series is then referred to as the SSTID index using the Kaplan SST dataset. The SSTID index is found to be correlated with the annual mean AMO index (Enfield *et al* 2001) ($r = 0.55$ for 1860–2011), indicating that the AMO makes some contribution to the SSTID, but a large fraction of the variance in the SSTID remains unexplained. Moreover, a rapid drop is clearly found in the annual SSTID index around 1970 with a very short timescale, and such an abrupt drop is not observed in the oscillatory multidecadal SST variations (e.g., the AMO). The SSTID shows contrasting positive and negative correlations in the NH and SH SST fields, respectively, in all large basins, with the most significant correlations observed in the Atlantic and Indian oceans (figure 2(b)). During the positive phase of SSTID, warming often appears in NH ocean basins, while the SH ocean basins are usually dominated by surface cooling. Enfield and Mestas-Nuñez (1999) conducted EOF analyses on the detrended, ENSO-removed global SSTA, and their EOF3 resembles the SSTID. However, in this study, the SSTID can be directly obtained as the EOF3 of zonal mean SSTA without any temporal filtering. The correlation patterns obtained using the HadISST and ERSST datasets are similar, indicating that the SST correlation pattern associated with SSTID is reliable. It is also worth noting that the global SST correlation pattern of SSTID differs significantly from that of the AMO, which only shows significant correlations in the North Atlantic region (Enfield *et al* 2001, Sutton and Hodson 2005).

Thompson *et al* (2010) identified an abrupt drop in the hemispheric differences in SST (NH minus SH) around 1970, and pointed that this drop derives not from oscillatory multidecadal SST variability. The SSTID index also shows a sudden shift from positive to negative around 1970. Furthermore, the SSTID index is highly correlated with NH minus SH SST ($r = 0.91$ based on annual mean data for 1860–2011). We performed the same analysis on the AMO index, but the correlation between the AMO and the hemispheric difference in SST is much lower ($r = 0.49$), indicating that the AMO is more representative of regional SST variations in the NH.

Latif *et al* (2006) and Keenlyside *et al* (2008) constructed the Atlantic SST dipole index to represent the latitudinally antisymmetric SST variations in the Atlantic, and used the index as an indicator of the Atlantic meridional overturning circulation (AMOC) variations. In this study, the SSTID is not confined is the Atlantic basin, as seen in figure 2(b). We then demonstrate the opposing SST polarity between the NH and SH in the SSTID. Because in the raw SSTA data, the in-phase relationship dominates between the NH and SH in terms of the EOF1 mode (global warming mode), we introduce the partial

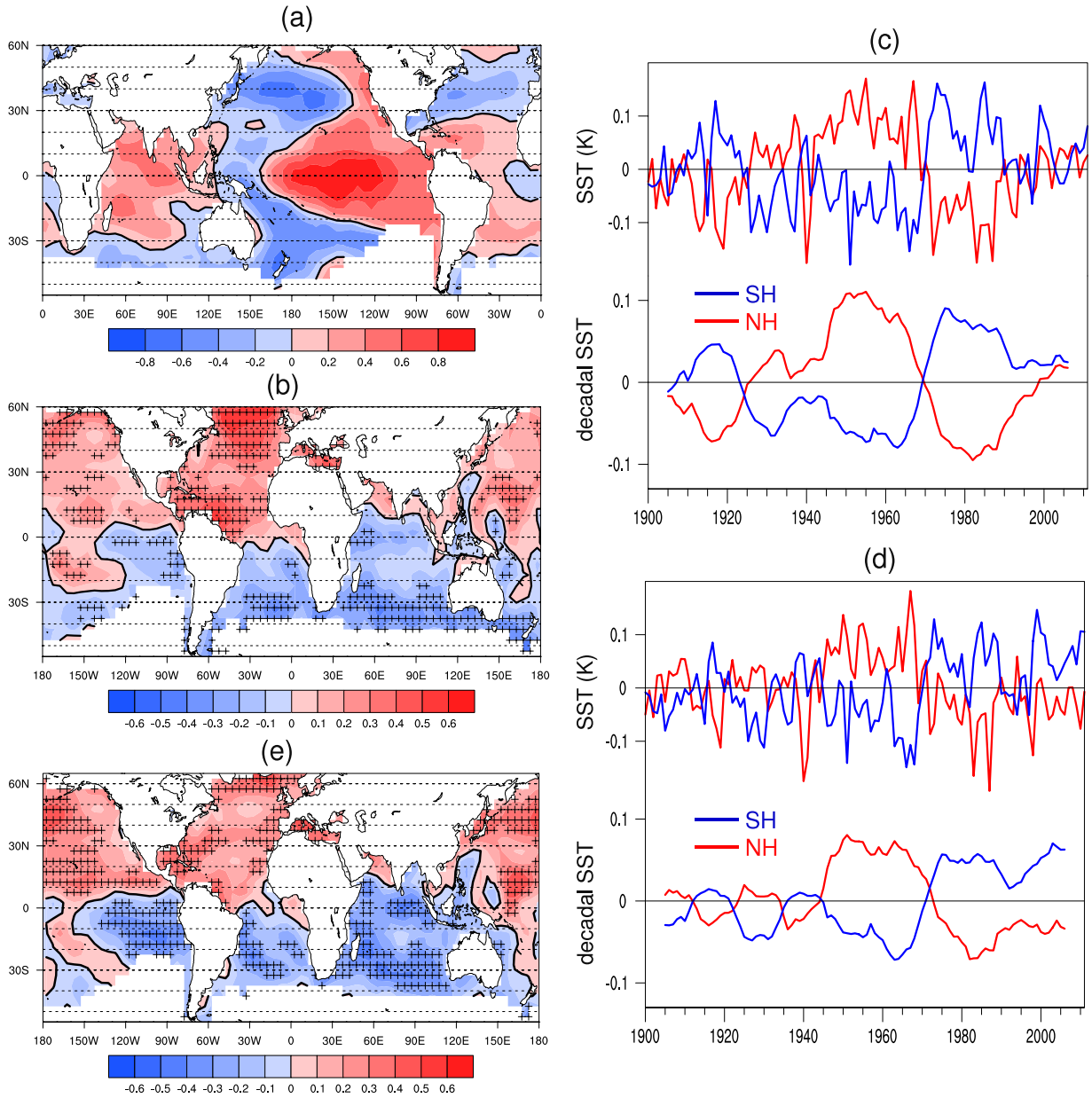

Figure 2. (a) Correlation map between the PC2 and global SSTA based on annual mean data from the Kaplan SST dataset (1900–2011). Black contours denote the zero line. (b) Same as in (a), but for the SSTID. (c) Annual mean time series (top) of residual SSTA (EOF1-removed) averaged poleward of 10° in the NH (red) and SH (blue) and their 11-yr running means (bottom). (d) Same as in (c), but for the residual SSTA time series with the AMO signal linearly removed. (e) Correlation of the NH averaged (poleward of 10°N) residual SSTA with the global residual SSTA based on the annual mean data (1900–2011) after removal of the AMO. In (b) and (e), areas marked by crosses are significant at the 95% confidence level.

correlation (Saji and Yamagata 2003) to remove the partial influence of EOF1 on the SSTA. Figure 2(c) shows the time series of residual SSTA averaged poleward of 10° in the NH and SH (where the amplitude of the SSTID is relatively large), and in some cases the positive values of NH SSTA coincide with negative SH SSTA and vice versa. Significant negative partial correlations (−0.55 for unfiltered data, −0.86 for 11-yr running means, both significant at the 95% confidence level) are found between the NH and SH averaged SSTA time series.

Furthermore, this antiphase relationship in the SSTID is almost independent of the AMO. The negative partial correlations (−0.42 for unfiltered data, −0.79 for 11-yr running means, both significant at the 95% confidence level) between NH and SH averaged SSTA (shown in figure 2(d)) remain after removal of the AMO signal (subtracting the regression onto the AMO index). Figure 2(e) further shows the partial correlation of the NH averaged (poleward of 10°N) residual SSTA with the global residual SSTA based on the data (1900–2011) after removal of the AMO signal. The contrasting positive and negative correlations in the NH and SH, respectively, are still evident in all large basins, and significant negative correlations can be observed in most part of the SH oceans. Moreover, SSTA over subtropical and northern North Atlantic regions are still found

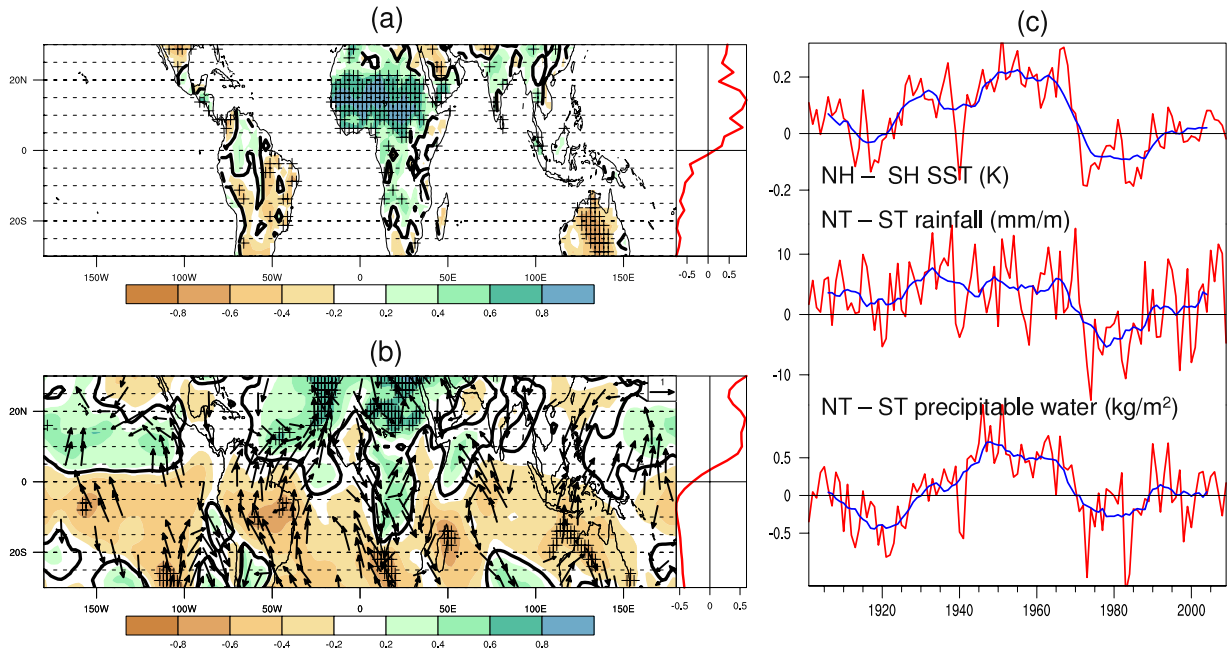

Figure 3. Connection between the SSTID and tropical rainfall on multidecadal timescales. (a) Correlation map between the SSTID index and tropical land precipitation (30°S–30°N) based on 11-yr running mean data over the period 1901–2009. Correlations for the zonal mean land precipitation with the SSTID index are shown as a red line. Black contours denote the zero line, and the areas marked by crosses are significant above the 95% confidence level. (b) Same as in (a), but for the precipitable water (shading and contours) and wind fields at 850 hPa (vectors). The arrows indicate wind correlations with the SSTID significant at the 95% confidence level. (c) Annual mean time series (red) of NH minus SH (NH–SH) raw SST for Kaplan dataset (top), NT minus ST (NT − ST) land precipitation (middle) and NT − ST precipitable water (bottom) over the period 1901–2009, and their 11-yr running means (blue). NT: 0°–30°N, ST: 30°S–0°.

to be significantly anticorrelated with the SH oceans. The northern North Atlantic region (above 50°N) is important for the NH and SH coupling. This region is considered capable of affecting the NH mean temperature due to the strong exchange of heat between the ocean and atmosphere (Knight *et al* 2005, Thompson *et al* 2010). In addition, the antiphase relationship between northern North Atlantic and SH temperatures has been identified from the paleoclimate records, and is explained by the bi-polar seesaw, which results from the inter-hemispheric redistribution of heat in response to the fluctuations in the North Atlantic deep water production (Broecker 1998, Stocker and Johnsen 2003).

3.2. SSTID and long-term variations in tropical precipitation

Figure 3 shows the influence of SSTID on decadal tropical rainfall variations over the period 1901–2009 and the underlying mechanisms. The rainfall-SST correlation (figure 3(a)) is not confined in the Sahel and Indian regions that are focused on in previous studies (Folland *et al* 1986, Knight *et al* 2006, Zhang and Delworth 2006). The correlation pattern mainly features a north–south dipole (positive and negative correlations in the NH and SH tropics, respectively) in terms of the zonal mean profile and horizontal distribution, although the positive correlations in Africa appear to extend south to the equator. To better evaluate this latitudinal asymmetry, the southern tropical (ST) mean land rainfall time series was subtracted from the northern tropical (NT) mean land rainfall time series (NT − ST rainfall) and the result is shown in figure 3(c). The time series of NT − ST rainfall exhibits interdecadal variability with a remarkably abrupt drop around 1970, and is simultaneously correlated with the SSTID index on decadal timescales ($r = 0.88$ for 11-yr running means). In particular, the recent recovery of the NT rainfall can be explained by the recent upward trend in the SSTID index. The correlation between the AMO and NT − ST rainfall is not statistically significant on multidecadal timescales ($r = 0.56$, not significant at the 95% confidence level), indicating that it is the global-scale SST variations that influence the latitudinal asymmetry of tropical rainfall, rather than the SST changes in a single basin. Therefore, these results provide observational evidence that the SSTID plays an important role in the north–south asymmetry of tropical precipitation.

The horizontal structure of atmospheric precipitable water correlated with the decadal SSTID index is shown in figure 3(b), and a north–south dipole is evident over most tropical regions except over the northeast Indian Ocean. The corresponding zonal mean profile shows correlations of opposite sign between the NH and SH tropics, basically consistent with the rainfall correlation. The moisture difference (NT − ST precipitable water, shown in figure 3(c)), like the precipitation field, shows strong multidecadal variability, and is simultaneously correlated with the SSTID index on multidecadal timescales ($r = 0.76$).

As mentioned in section 3.1, the SSTID is highly correlated with the raw SST difference between the NH and SH (shown in figure 3(c)). During the positive phase

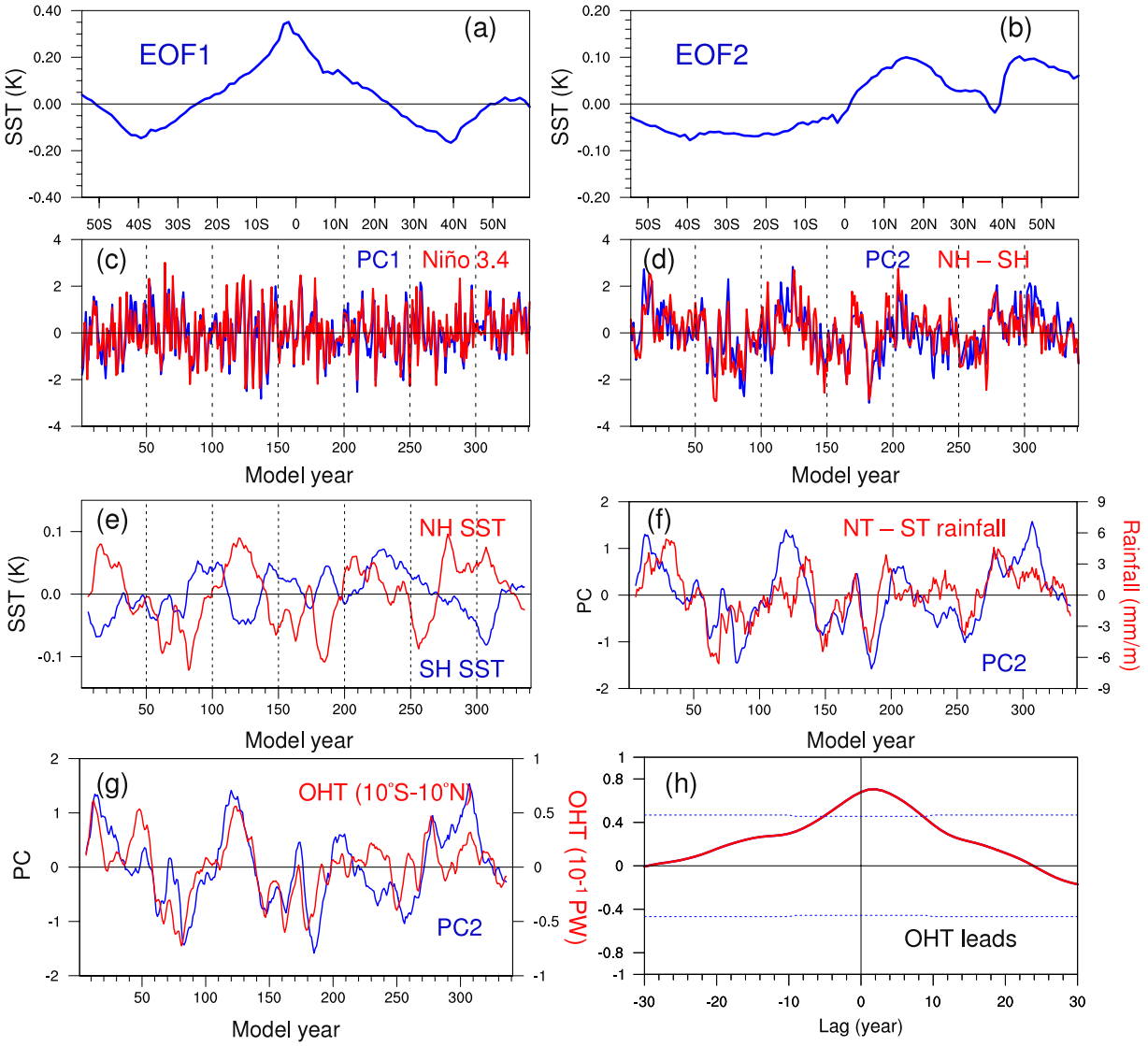

Figure 4. Simulated results in the UKMO-HadCM3 climate model. The first (a) and second (b) EOFs of the annual zonally averaged SSTA, shown as regressions of the SSTA onto the normalized EOF time series (PCs). (c) The normalized PC1 (blue) and Niño 3.4 SSTA (red). (d) The normalized PC2 (blue) and NH minus SH SSTA (red). (e) Annual mean time series of residual SSTA (after removing the effect of EOF1) averaged poleward of 10° in the NH (red) and SH (blue), shown as the 11-yr running means. (f) 11-yr running means of the normalized PC2 (blue) and the NT − ST precipitation (red). (g) 11-yr running means of the normalized PC2 (blue) and the global northward OHT across the equator (anomalies averaged between 10°S and 10°N, red, 1 PW = 10^{15} W). (h) Cross-correlations of the simulated SSTID (EOF2) with the global northward cross-equatorial OHT. Positive lags mean that the OHT is leading, and the blue dashed lines denote the 95% confidence level.

of the SSTID, the NH tropical SST is often warmer than that in the SH tropics, as seen in the latitudinal pattern of SSTID, and this northward SST gradient near the equator can influence moisture distribution in two ways. First, theoretical and observational analyses have demonstrated that the northward SST gradient is favorable for anomalous low-level southerlies in the tropical region (Lindzen and Nigam 1987, Feng *et al* 2011, 2013). As shown in figure 3(b), the observed correlation pattern between the decadal SSTID index and low-level wind field shows significant cross-equatorial southerlies over most equatorial regions, and particularly over the Atlantic and Indian Ocean basins. These anomalous southerlies can result in a northward moisture transport, which generates the moisture increase and decrease in the NH and SH tropics, respectively. Second, higher SST in the NH tropics than in the SH tropics may give the low-level atmosphere a higher moisture holding capability, because of the Clausius–Clapeyron relationship (Held and Soden 2006), this also contributes to the northward gradient in the moisture.

3.3. Simulated results in UKMO-HadCM3

Figure 4 shows the leading two EOFs of the annual zonally averaged SSTA in the UKMO-HadCM3 simulations. The variability of zonal mean SSTA is mainly explained by one equatorially symmetric mode and one antisymmetric mode, which account for 43% and 17% of the total variance,

respectively. The latitudinal patterns of these two modes are similar to the EOF2 and EOF3 (or SSTID) in the observations. The interpretations of the simulated EOF1 and EOF2 are further investigated. The PC1 is dominated by interannual variability and shown to be strongly correlated with the annual Niño 3.4 SSTA in the simulations ($r = 0.82$, significant at the 95% confidence level), suggesting that the EOF1 can be largely explained by the ENSO signature. The correlation of the simulated EOF2 with the EOF for the SSTID mode in Kaplan dataset is strong ($r = 0.90$). The correlation between the simulated PC2 and the inter-hemispheric thermal gradient (NH minus SH SST) is high and significant ($r = 0.80$). Moreover, the partial correlation between the NH and SH mean (poleward of 10°) SSTA time series (after removing the effect of EOF1) is significantly negative ($r = -0.43$ for 11-yr running means), confirming the inter-hemispheric dipole-like SST pattern in the SSTID. Therefore, these results suggest that the observed SSTID is realistically reproduced in the UKMO-HadCM3 control simulations. We also examine the correlation between the SSTID and tropical rainfall on decadal timescales (figure 4(f)), and they are basically in phase with each other ($r = 0.70$, significant at the 95% confidence level), indicating that the observed relationship between the SSTID and tropical rainfall is considerably well simulated by the UKMO-HadCM3 climate model.

We further use the simulations to investigate the possible physical process controlling the variations in the SSTID. A tight connection is found between the SSTID and the global northward ocean heat transport (OHT) across the equator (figure 4(g)). Moreover, as shown by the lead–lag correlation between the northward cross-equatorial OHT and the SSTID (figure 4(h)), the OHT appears to lead the SSTID by several years, indicating that fluctuations in the SSTID are primarily driven by the changes in the OHT. Previous modeling studies have suggested that an enhanced northward cross-equatorial OHT corresponds to a net transfer of heat from the SH to the NH and thus can induce anomalous warming in the NH oceans and cooling in the SH oceans, exhibiting a dipole SST anomaly similar to the SSTID pattern (Vellinga and Wood 2002, Zhang and Delworth 2005, Marshall *et al* 2013). Thus, the SSTID found in this study may be interpreted as a SST mode physically related to the variability of the global cross-equatorial OHT.

4. Summary and discussion

In the present study, the long-term variability of latitudinal SST fluctuations was investigated in terms of zonal mean SSTA using three different SST datasets (Kaplan, HadISST and ERSST). Besides the global warming mode, the variability is dominated by an equatorially symmetric mode and an antisymmetric mode. The former mode is mainly over the Pacific basin, and shows interannual timescales, corresponding to the ENSO signature. The latter mode features an inter-hemispheric dipole-like SST pattern with centers of action prevailing over the Atlantic and Indian Ocean basins, and is therefore referred to as the SST inter-hemispheric dipole (SSTID). The SSTID is partially associated with the AMO as suggested by previous studies (Enfield and Mestas-Nuñez 1999, Parker *et al* 2007), but it differs from the AMO in the spatial pattern. The SSTID is strongly correlated with the variations in the inter-hemispheric thermal gradient, and therefore it significantly influences the tropical rainfall and drives the north–south asymmetry of tropical precipitation on multidecadal timescales. The UKMO-HadCM3 climate model can well show the observed SSTID and its relation to the tropical precipitation, and furthermore, the simulated SSTID is found to be physically related to the variability of the global cross-equatorial OHT.

There are still some interesting questions to be answered. Modeling studies have suggested that the AMOC plays an essential role in the global cross-equatorial OHT, affecting the heat partitioning between the two hemispheres (Vellinga and Wood 2002, Zhang and Delworth 2005). Thus, further studies are required on the possible relationship between the Atlantic SST dipole (Latif *et al* 2006), the AMOC, and the SSTID and the possible mechanistic difference between the AMO and the SSTID, which may help us understand the physical mechanism for the formation and evolution of the SSTID. In addition, we have focused on the variability of latitudinal SST fluctuations using annual mean data, the space–time features of this variability during different seasons are still open to further investigation.

Acknowledgments

The authors wish to thank two anonymous reviewers for their constructive comments. This work was jointly supported by the 973 Program (2010CB950400), the NSFC Projects 41290255 and 41175069, and the Climate Change Special Project of the State Ocean Administration.

References

Alexander M A, Blade I, Newman M, Lanzante J R, Lau N C and Scott J D 2002 The atmospheric bridge: the influence of ENSO teleconnections on air–sea interaction over the global oceans *J. Clim.* **15** 2205–31

Baines P G and Folland C K 2007 Evidence for a rapid global climate shift across the late 1960s *J. Clim.* **20** 2721–44

Broecker W S 1998 Paleocean circulation during the last deglaciation: a bipolar seesaw? *Paleoceanography* **13** 119–21

Compo G P *et al* 2011 The twentieth century reanalysis project *Q. J. R. Meteorol. Soc.* **137** 1–28

Deser C, Alexander M A, Xie S-P and Phillips A S 2010 Sea surface temperature variability: patterns and mechanisms *Annu. Rev. Mar. Sci.* **2** 115–43

Dima M and Lohmann G 2010 Evidence for two distinct modes of large-scale ocean circulation changes over the last century *J. Clim.* **23** 5–16

Drost F, Karoly D and Braganza K 2012 Communicating global climate change using simple indices: an update *Clim. Dyn.* **39** 989–99

Enfield D B and Mestas-Nuñez A M 1999 Multiscale variabilities in global sea surface temperatures and their relationships with tropospheric climate patterns *J. Clim.* **12** 2719–33

Enfield D B, Mestas-Nuñez A M and Trimble P J 2001 The Atlantic multidecadal oscillation and its relation to rainfall and river flows in the continental US *Geophys. Res. Lett.* **28** 2077–80

Feng R, Li J P and Wang J C 2011 Regime change of the boreal summer Hadley circulation and its connection with the tropical SST *J. Clim.* **24** 3867–77
Feng J, Li J P and Xie F 2013 Long-term variation of the principal mode of boreal spring Hadley circulation linked to SST over the Indo-Pacific warm pool *J. Clim.* **26** 532–44
Folland C K, Palmer T N and Parker D E 1986 Sahel rainfall and worldwide sea temperatures, 1901–85 *Nature* **320** 602–7
Folland C K, Parker D E, Colman A W and Washington R 1999 Large scale modes of ocean surface temperature since the late nineteenth century *Beyond El Niño: Decadal and Interdecadal Climate Variability* ed A Navarra (Berlin: Springer) pp 73–102
Gordon C, Cooper C, Senior C A, Banks H, Gregory J M, Johns T C, Mitchell J F B and Wood R A 2000 The simulation of SST, sea ice extents and ocean heat transports in a version of the Hadley centre coupled model without flux adjustments *Clim. Dyn.* **16** 147–68
Guilyardi E, Wittenberg A, Fedorov A, Collins M, Wang C Z, Capotondi A, van Oldenborgh G J and Stockdale T 2009 Understanding El Nino in ocean–atmosphere general circulation models progress and challenges *Bull. Am. Meteorol. Soc.* **90** 325–40
Held I M and Soden B J 2006 Robust responses of the hydrological cycle to global warming *J. Clim.* **19** 5686–99
Kaplan A, Cane M A, Kushnir Y, Clement A C, Blumenthal M B and Rajagopalan B 1998 Analyses of global sea surface temperature 1856–1991 *J. Geophys. Res.* **103** 18567–89
Keenlyside N S, Latif M, Jungclaus J, Kornblueh L and Roeckner E 2008 Advancing decadal-scale climate prediction in the North Atlantic sector *Nature* **453** 84–8
Knight J R, Allan R J, Folland C K, Vellinga M and Mann M E 2005 A signature of persistent natural thermohaline circulation cycles in observed climate *Geophys. Res. Lett.* **32** L20708
Knight J R, Folland C K and Scaife A A 2006 Climate impacts of the Atlantic multidecadal oscillation *Geophys. Res. Lett.* **33** L17706
Latif M, Boning C, Willebrand J, Biastoch A, Dengg J, Keenlyside N, Schweckendiek U and Madec G 2006 Is the thermohaline circulation changing? *J. Clim.* **19** 4631–7
Li Y, Li J P and Feng J 2012 A teleconnection between the reduction of rainfall in southwest western Australia and north China *J. Clim.* **25** 8444–61
Lindzen R S and Nigam S 1987 On the role of sea-surface temperature-gradients in forcing low-level winds and convergence in the tropics *J. Atmos. Sci.* **44** 2418–36
Marshall J, Donohoe A, Ferreira D and McGee D 2013 The ocean's role in setting the mean position of the inter-tropical convergence zone *Clim. Dyn.* doi:10.1007/s00382-013-1767-z
Mitchell T D and Jones P D 2005 An improved method of constructing a database of monthly climate observations and associated high-resolution grids *Int. J. Climatol.* **25** 693–712
North G R, Bell T L, Cahalan R F and Moeng F J 1982a Sampling errors in the estimation of empirical orthogonal functions *Mon. Weather Rev.* **110** 699–706
North G R, Moeng F J, Bell T L and Cahalan R F 1982b The latitude dependence of the variance of zonally averaged quantities *Mon. Weather Rev.* **110** 319–26
Parker D, Folland C, Scaife A, Knight J, Colman A, Baines P and Dong B 2007 Decadal to multidecadal variability and the climate change background *J. Geophys. Res.* **112** D18115
Quadrelli R, Bretherton C S and Wallace J M 2005 On sampling errors in empirical orthogonal functions *J. Clim.* **18** 3704–10
Rayner N A, Brohan P, Parker D E, Folland C K, Kennedy J J, Vanicek M, Ansell T J and Tett S F B 2006 Improved analyses of changes and uncertainties in sea surface temperature measured *in situ* since the mid-nineteenth century: the HadSST2 dataset *J. Clim.* **19** 446–69
Saji N H and Yamagata T 2003 Structure of SST and surface wind variability during Indian ocean dipole mode events: COADS observations *J. Clim.* **16** 2735–51
Smith T M and Reynolds R W 2004 Improved extended reconstruction of SST (1854–1997) *J. Clim.* **17** 2466–77
Stocker T F and Johnsen S J 2003 A minimum thermodynamic model for the bipolar seesaw *Paleoceanography* **18** 1087
Sutton R T and Hodson D L R 2005 Atlantic Ocean forcing of North American and European summer climate *Science* **309** 115–8
Thompson D W J, Wallace J M, Kennedy J J and Jones P D 2010 An abrupt drop in Northern Hemisphere sea surface temperature around 1970 *Nature* **467** 444–7
Ting M F, Kushnir Y, Seager R and Li C H 2009 Forced and internal twentieth-century SST trends in the North Atlantic *J. Clim.* **22** 1469–81
Vellinga M and Wood R A 2002 Global climatic impacts of a collapse of the Atlantic thermohaline circulation *Clim. Change* **54** 251–67
Xu Y Y and Ramanathan V 2012 Latitudinally asymmetric response of global surface temperature: implications for regional climate change *Geophys. Res. Lett.* **39** L13706
Zhang R and Delworth T L 2005 Simulated tropical response to a substantial weakening of the Atlantic thermohaline circulation *J. Clim.* **18** 1853–60
Zhang R and Delworth T L 2006 Impact of Atlantic multidecadal oscillations on India/Sahel rainfall and Atlantic hurricanes *Geophys. Res. Lett.* **33** L17712
Zhang R *et al* 2013 Have aerosols caused the observed Atlantic multidecadal variability? *J. Atmos. Sci.* **70** 1135–44
Zhang Y, Wallace J M and Battisti D S 1997 ENSO-like interdecadal variability: 1900–93 *J. Clim.* **10** 1004–20